Korean J. of Chem. Eng., **6**(2) (1989) *112-120*

SIMULATION OF THE NEWTONIAN FLOW THROUGH AN ABRUPTLY CONTRACTED TUBE USING A MIXED FINITE ELEMENT METHOD

Jung Do HUH, Pan Wook PARK*, and Young Ok JUNG**

Department of Chemical Engineering, Pohang Institute of Science and Technology,
P.O. Box 125, Pohang 790-600, Korea
*Department of Chemical Engineering, Pusan National University
**Department of Chemical Engineering, Pusan National Open University
(Received 4 May 1988 • accepted 21 September 1988)

Abstract—The solutions of the Navier-Stokes equation for a Newtonian flow through a 4/1 contraction tube were obtained numerically using the Galerkin finite element method with the nine-node Lagrangian element which was believed to be one of the most accurate tools for mixed-type interpolating formulations. It was proved from this study that the vortex occurrence in the entrance corner region were confirmed but its size was gradually decreased with the increase of Reynolds numbers, and that the velocity profiles and pressure distributions along the applied mesh layers were in agreement with the experimental and the previously reported numerical results.

INTRODUCTION

In the analysis of the incompressible fluid through a contraction tube, the mixed finite element method (FEM) has appeared as a relevant and powerful tool for solving the Navier-Stokes equations. Recently, a stable, accurate, and economic finite element method has been searched for the nonlinear steady-state system coupled with Convection-Diffusion-Reaction terms, such as a tubular reactor design and a chemical process control. The analysis of complex flow problems can be performed by one of three alternative formulations, that is, the velocity-pressure, the stream function-vorticity, and the stream function formulation. In this study, the velocity-pressure formulation is mainly used for its popularity and convenience to treat.

Concerning the FEM which has been adopted for solutions of Navier-Stokes equations, difficulty arises in formulating the discretization of governing equations and in selecting the appropriate interpolating functions for velocity and pressure variables. In this respect, Huyakorn et al. [1] compared four types of quadrilateral elements in terms of the accuracy of interpolation and showed that the nine-node Lagrangian element gave the most accurate pressure and velocity distributions. On the other hand, as recognized by Kawahara and Takeuchi [2] and others [3-5], the mixed finite element Galerkin approach seemed most convenient to discretize governing equations describing complex flow problems.

The numerical simulation of the fluid flow through a sudden contraction tube has been examined by Vrentas and Duda [6,7] and other research groups [8-10]. The important aspects of circular entry flows, including an abrupt contraction problem, were recently reviewed in Boger's article [11]. Discussions made in this review article mainly concern the intensity and size of the recirculating vortex and the extra pressure loss, or the Couette correction, due to the sudden contraction. In Newtonian flow analysis, most of studies reported that streamlines, vorticity distributions, velocity profiles, excess pressure drops, and entrance lengths may be evaluated as functions of Reynolds number and radius ratio.

In the present work, we develop solutions of primitive Navier-Stokes equations governing a Newtonian fluid through a 4/1 contraction tube by employing the mixed FEM with the nine-node Lagrangian quadrilateral elements. Then, results obtained from this study are compared with the experimental and other numerical results in terms of velocity profiles, pressure distributions, and vortex behaviors with Reynolds number.

To whom all correspondence should be addressed.

FORMULATION OF EQUATION

1. Basic equations

Consider the isothermal, laminar flow of an incompressible Newtonian fluid through a cylindrical and axisymmetric contraction tube, as shown in Fig. 1. The contraction tube is of radius R extending from $z = z_1$ to $z = 0$ connected to a smaller tube of radius R/4 which extends from $z = 0$ to $z = z_2$.

For the steady-state, axisymmetric, isothermal flow of a Newtonian fluid with a constant viscosity, the dimensionless equations of motion in cylindrical coordinates are given as

z-component:

$$V_r V_{z,r} + V_z V_{z,z} = -P_{,z} + [(rV_{z,r})_{,r}/r + V_{z,zz}]/Re + g_z \quad (1a)$$

r-component:

$$V_r V_{r,r} + V_z V_{r,z} = -P_{,r} + [(rV_r)_{,r}/r)_{,r} + V_{r,zz}]/Re + g_r \quad (1b)$$

where V_r and V_z represent the radial and the axial velocity components in cylindrical coordinates. P indicates the pressure and g the gravitational constant. In above equations, subscripts ',r' and ',z' denote first-order derivatives with respect to r and z, and the subscript ',zz' the second-order derivative with respect to z. In this coordinate system, the equation of continuity can be shown to be

$$(rV_r)_{,r}/r + V_{z,z} = 0. \quad (1c)$$

In order to discretize the Eq.(1) for the domain of the flow field, a mixed finite element procedure may be employed. By the method of weighted residuals, the formulation of the usual Galerkin weak solution yields V_r, V_z, and P as follows.

For the axial velocity component:

$$2\pi \int_\Omega dr\,dz [V_z^* (V_r V_{z,r} + V_z V_{z,z})r - V_{z,z}^* rP + V_{z,z}^* (V_{z,r} + V_{z,z})r/Re]$$
$$= 2\pi \int_\Omega V_z^* g_z r\,dr\,dz - 2\pi L \int_{\Gamma_z} V_z^* P n_z r\,dr + (2\pi R/Re) \int_{\Gamma_r} V_z^* V_{z,r} n r\,dz + (2\pi L/Re) \cdot \int_{\Gamma_z} V_z^* V_{z,z} n_z r\,dr \quad (2a)$$

For the radial velocity component:

$$2\pi \int_\Omega dr\,dz [V_r^* (V_r V_{r,r} + V_z V_{r,z})r - (rV_r^*)_{,r} P + (rV_r^*)_{,r} (rV_r)_{,r}/rRe + V_{r,z}^* V_{r,z} r/Re]$$
$$= 2\pi \int_\Omega V_r^* g_r r\,dr\,dz - 2\pi R \int_{\Gamma_r} V_r^* P n_r\,dz + (2\pi R/Re) \int_{\Gamma_r} V_r^* (rV_r)_{,r} n r\,dz + (2\pi L/Re) \cdot \int_{\Gamma_z} V_r^* V_{r,z} n_z r\,dr \quad (2b)$$

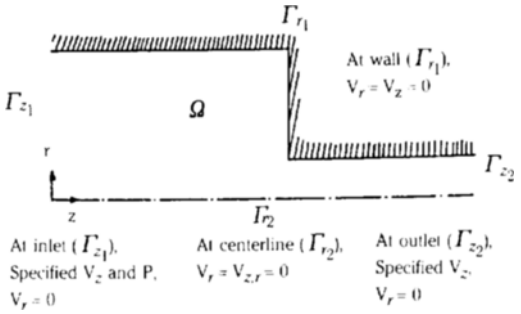

Fig. 1. A Schematic diagram of the axisymmetric region and the illustration of boundary conditions.

For the pressure:

$$2\pi \int_\Omega P^* (rV_r)_{,r}\,dr\,dz + 2\pi \int_\Omega P^* V_{z,z} r\,dr\,dz = 0 \quad (2c)$$

where the superscript * indicates the weighting function.

As shown in Fig. 1, a set of the notation Γ represents the boundary of the flow field under consideration. Γ_r corresponds to conditions at wall and at centerline, and Γ_z to conditions of the entry and the exit of the tube. The total tube length including the contraction part is denoted by L.

In order to solve above equations, a set of suitable boundary conditions for each given boundary Γ has to be chosen like the ones illustrated in Fig. 1. These are shown below in detail:

$$V_r = 0,\ V_z = V_z(r),\ P = P_o \quad \text{on } (r, z) \in \Gamma_{z_1} \quad (3a)$$
$$V_r = V_z = 0 \quad \text{on } (r, z) \in \Gamma_{r_1} \quad (3b)$$
$$V_r = V_{z,r} = 0 \quad \text{on } (r, z) \in \Gamma_{r_2} \quad (3c)$$
$$V_z = V_z(r),\ V_{r,z} = 0 \quad \text{on } (r, z) \in \Gamma_{z_2}. \quad (3d)$$

Under these conditions all boundary integral terms in weighted residual equations, Eqs. 2(a)-2(c), become to vanish at once so that computation can be done in more simplified manner.

2. Numerical simulation

The next procedure to derive a set of algebraic equations from Eq.(2) may be drawn from previous works [1,12,13]. The nine-node element shown in Fig. 2 is a mixed-type interpolation which is composed of quadratic shape functions for velocities, and of linear shape functions for a pressure. This is a natural choice of interpolating functions when we recognize the presence of the second-order derivatives of velocities but only the first-order derivatives for the pressure in

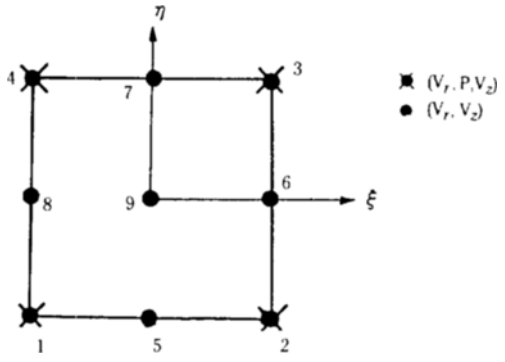

Fig. 2. A mixed interpolation element (a nine-node Lagrangian element).

Eq.(1).

Thus, velocities and a pressure can be approximated using interpolating shape functions like below.

$$V_i^e(r,z)=\sum_{\alpha=1}^{9}\phi_\alpha^e(r,z)V_i,\quad V_i^*(r,z)=\phi_\alpha^e(r,z) \tag{4a}$$

$$P^e(r,z)=\sum_{\beta=1}^{4}\theta_\beta^e(r,z)P,\quad P^*(r,z)=\theta_\beta^e(r,z) \tag{4b}$$

where the superscript e indicates an element under consideration and α and β are nodal points of the element. Here, ϕ_α and θ_β represent a nine-node biquadratic function and a four-node bilinear shape function, respectively.

By substituting Eq.(4) into Eq.(2), residual equations for an element are obtained in integral forms. These integrals should be evaluated over the standard element shown in Fig. 2. A Newton-Raphson iteration scheme requires the formulation of the Jacobian matrix to solve nonlinear residual equations. First of all, the element Jacobian matrix can be derived by differentiating each residual vector with respect to system variables which are the axial and the radial velocities, and the pressure.

Integral expressions shown in element residual equations and the element Jacobian matrix are usually evaluated by the use of the numerical integration method known as the Gaussian quadrature. By the quadrature rule, integration is approximated to weighted summation over all applying quadrature points. This is a well-known method in the conventional FEM analysis.

Consequently, all residual and Jacobian forms of equations can be computed numerically over the element by the just mentioned rule. It follows that contributions of residual vectors of each element in the system are simply assembled element by element to form a whole system residual vector,

$$R(\psi)=0. \tag{5}$$

Now, it is possible to set up the numerical scheme to solve our system of nonlinear equations, Eq.(5). The well-known Newton-Raphson method to treat nonlinearity has been selected and described below by using vector notations.

$$J(\psi_n)\cdot\Delta\psi_n=R_n \tag{6a}$$

$$\psi_{n+1}=\psi_n+\Delta\psi_n \tag{6b}$$

where the subscript n is the iteration number and ψ is the unknown vector to be solved. This method has a quadratic convergence which is considered to be fast compared to other iteration methods, but unfortunately it has a serious drawback which requires a good initial guess to start iteration with.

It is noted in Eq.(6a) that an efficient linear equation solver is needed to save the computation time and to reduce computer memory capacity, due to the inversion of the huge Jacobian matrix. In this respect, the unsymmetrical version of 'frontal method' developed by Hood [14] has been employed to our problem. It has been proved in the literature that this method saves much of the core memory because the computer needs to memorize variables corresponding to only the one short side of the geometry instead of a whole system of variables.

As a termination criterion of the Newton-Raphson iteration, we take the form of the standard deviation (δ) between two consecutive solutions:

$$\delta=[\Sigma_i(\psi_i-\psi_{i-1})^2/\Sigma_i\psi_i\cdot\psi_i]^{1/2}<10^{-6} \tag{7}$$

For the case of Re = 1.0, four iteration steps were needed to satisfy the above convergence criterion and six steps were sufficient for Re = 10.0.

RESULTS AND DISCUSSION

1. Elemental mesh analysis

Applying the nine-node Lagrangian element to the confined geometry of a 4/1 contraction tube, we compose meshes which are concentrated to the sharp edge of contraction. The sharp edge point P in the Fig. 3 shows a geometrically singular behavior. That is, it involves the drastic change in their magnitudes of variables in solving the Navier-Stokes equation. Thus, in order to avoid this difficulty, we adopt the specially refined meshes near the point P as represented in the Fig. 3 (The dotted box in Fig. 3 represents magnification of the mesh refinement in that particular region). By using six nine-node Lagrangian elements in vertical placement and by confining the tube length from z = -4.8 to z = 1.35 in the axial direction, our problem contains 1078 nodes, 252 elements, and 2452 unknowns (or algebraic equations).

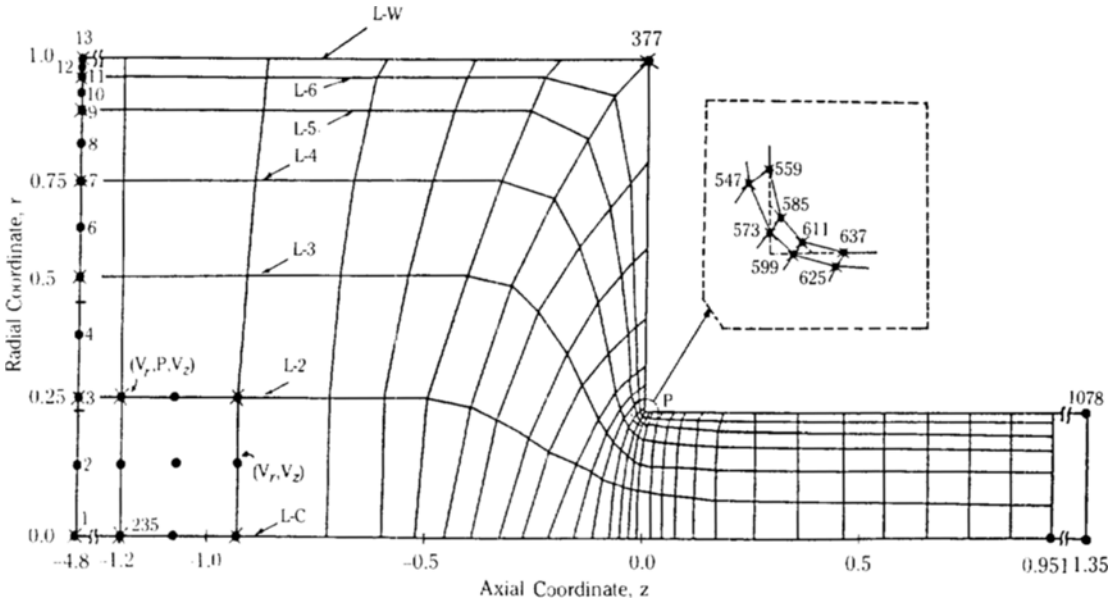

Fig. 3. Finite element meshes, mesh layers (L-C, L-2, etc.), and nodes for a Newtonian fluid through the 4/1 contraction tube (✱ V_r, V_z, P: ● V_r, V_z) with 252 elements, 1078 nodes, and 2452 unknowns.

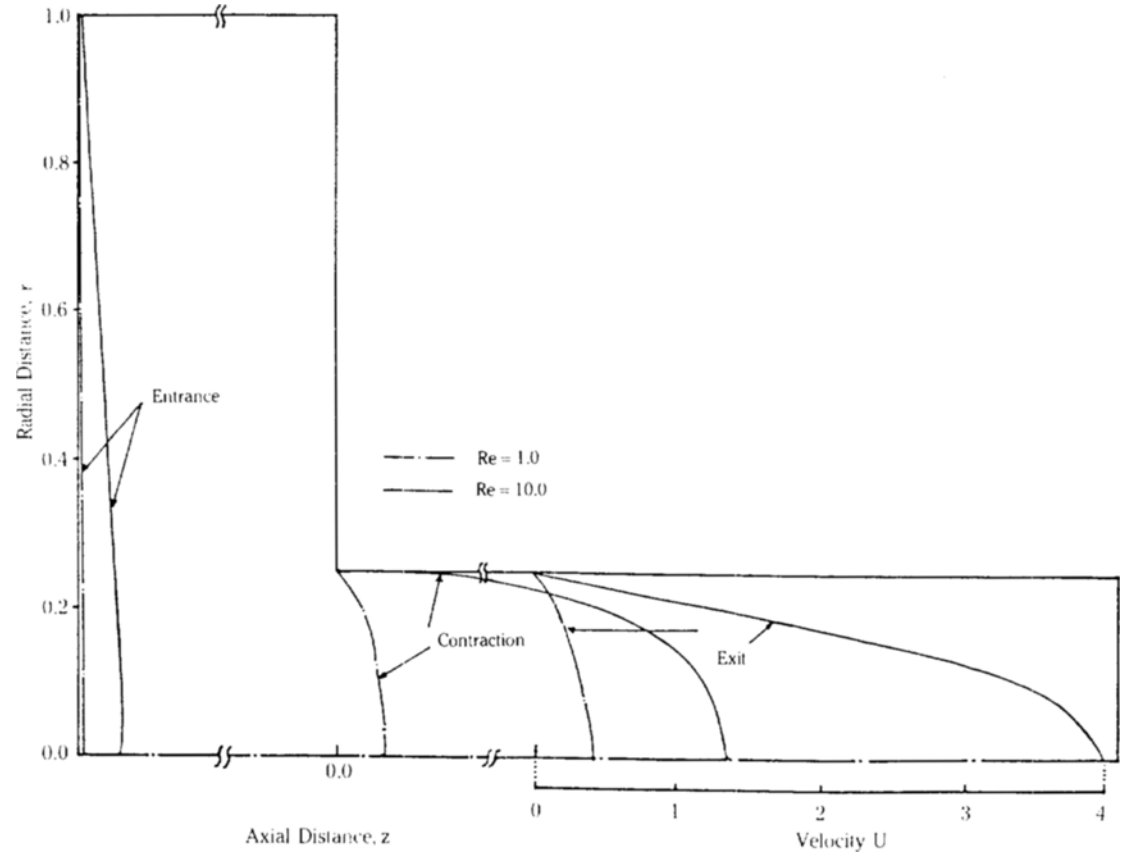

Fig. 4. Velocity profiles across the tube for Re = 1.0 and 10.

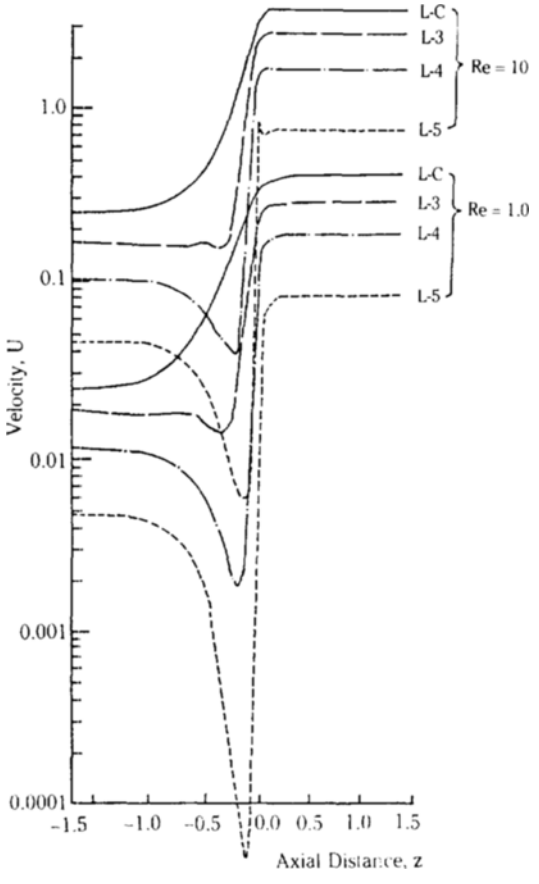

Fig. 5. Velocity distributions along the axis for mesh layers for Re = 1.0 and 10.

In order to investigate the flow behavior in the tube, mesh layers are classified into L-C, L-2, ..., L-W, counting from the centerline of the tube toward the wall in which the interval between layers becomes shorter near the wall due to sharp variations of variables taking place there. These mesh layers are basically used to demonstrate the velocity profile and the pressure distribution changing with radial positions. Reynolds number were also changed to show its influence on flow velocities and vorticities. To observe the pressure drop and velocity profiles due to the entrance effect of the sudden contraction region, the origin of the axial coordinates is located at the reentrance point.

2. Velocity profiles and vortex occurrences

Fig. 4 shows the relation of velocity profiles with Reynolds number in the 4/1 contraction tube. The velocity at the centerline of the tube rapidly increases when the flow goes through the contraction point, $z = 0$, and then remains constant, but it is still far greater than that of the upstream. Also, it can be reaffirmed that the increase of the fluid velocity (or Reynolds number) accelerates the effect of contraction.

The velocity distribution along various layers at Re = 1.0 and at Re = 10 are depicted in Fig. 5. Except the L-C layer, the substantial decrease of the velocity just before the abruptly contracted point $z = 0$ must be the evidence of occurrences of the vorticity in the corner. Closer to the wall is the location, more decrease in the velocity field has been found to indicate the onset of a vorticity. It has been shown that effects of the vortex occurrence, however, have been decreased with the increase of Reynolds number or the velocity. The convective force of the flow from the upstream due to high Reynolds number is believed to suppress the activity of the vortex and to reduce its magnitude. The sharp rise of the velocity just after $z = 0$ may be explained by the consequence of 4/1 contraction of the tube.

Velocity contours and vortex behaviors in the corner region are shown with Re in Fig. 6. For cases of Figs. 6(a) and 6(b), the arrow which represents the velocity vector at each nodal point is lengthened according to the magnitude and slanted to lead each flow direction. In these figures the strength of the vorticity must be weak enough to be seen by short arrow signs, as expected. Note that eddies in the corner regions are diminished in size and in strength as the flow of the higher Reynolds number is approached. In addition, velocities arriving at the entrance corner is found to be enlarged in a great amount and is directed to the downward against the pressure generated by the parallel flow at the entrance.

The above results of the present study are consistent with previous investigations [6,15,16] although the existence of vortices could be more visually detected by using the stream function description instead of the velocity vector representation used in this study.

The comparison of these velocity vectors and vortex occurrences for different Re with experimental data of creeping flows [16] and other numerical solutions [10,11], is shown in Fig. 7. The entry pattern observed for the Newtonian viscous flow [16] which is the typical creeping flow is shown on the upper picture of Fig. 7(a). The flow is almost radial, with only a small secondary flow existing in the corner of the upstream tube, which is properly consistent with the velocity and the vorticity pattern on the lower picture of Fig. 7(a) obtained from the simulation of this work. The same conclusion may be drawn from Fig. (b) for Re = 10, which depicts both simulation results of the present work (on the upper) and those of Boger [11].

3. Pressure distribution

Figs. 8(a) and 8(b) are shown to illustrate our computational results of the pressure distribution near the

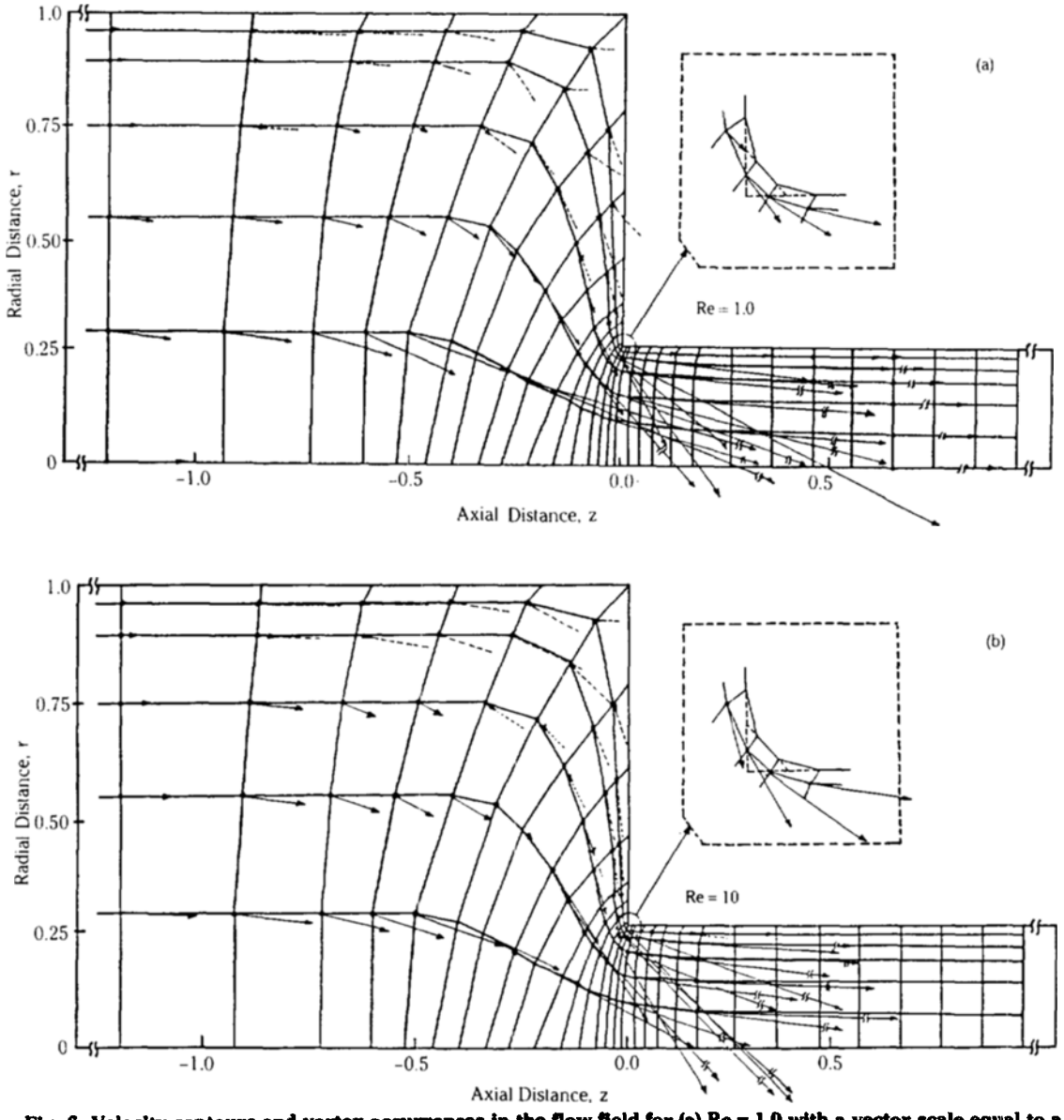

Fig. 6. Velocity contours and vortex occurrences in the flow field for (a) Re = 1.0 with a vector scale equal to a hundred time of computed values and (b) Re = 10 with a vector scale equal to ten times of computed values.

contraction. In this plot, the abscissa represents the dimensionless axial distance in which positive numbers are the indication of the small tube, while the negatives are of the large tube.

Comparing these figures, the pressure rise due to collision of the flow from the upstream against the contraction wall is clearly demonstrated to be higher with the lower Reynolds number. This may be conjectured that viscous flows with the low Reynolds number usually develop a full flow pattern, which implies the adaptation of the flow to the given obstacle, in much slower fashion than the relatively high Reynolds number so that before the former makes its full pattern according to the geometry encountered, it will hit the barrier to produce the higher wall pressure than the latter of the more developed case.

It is also noted from Figs. 8(a) and 8(b) that the node of the maximum pressure rise changes with Rey-

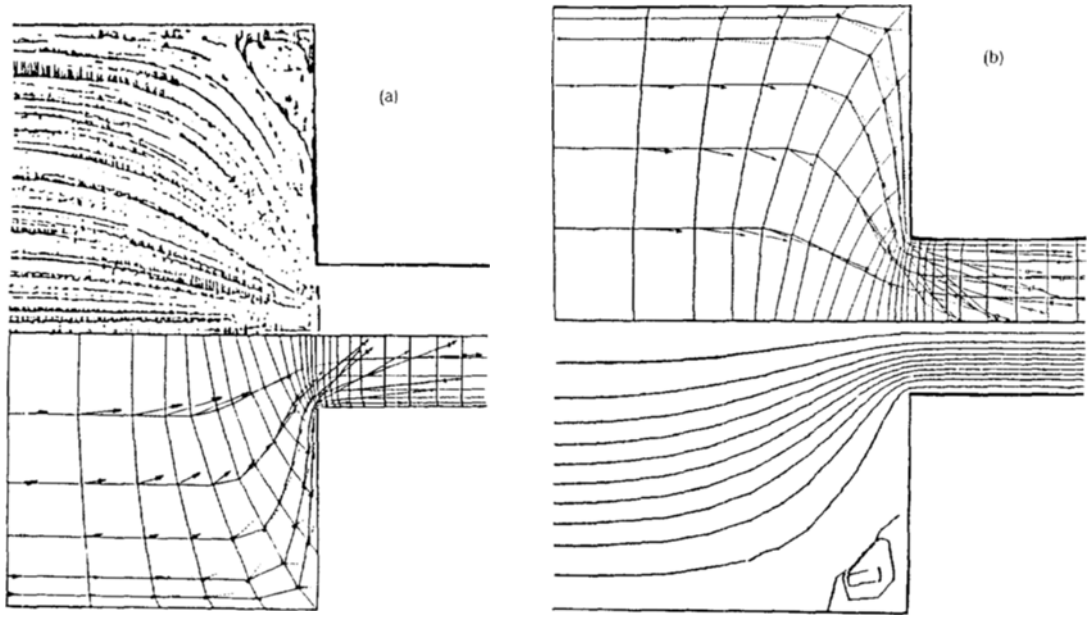

Fig. 7. Comparisons of velocity vectors of numerical solutions for a Newtonian flow in a 4/1 contraction: (a) for Re = 1.0 on the lower and experimental data of creeping flow [17] on the upper and (b) for Re = 10 on the upper and a numerical solution of Boger [11] on the lower.

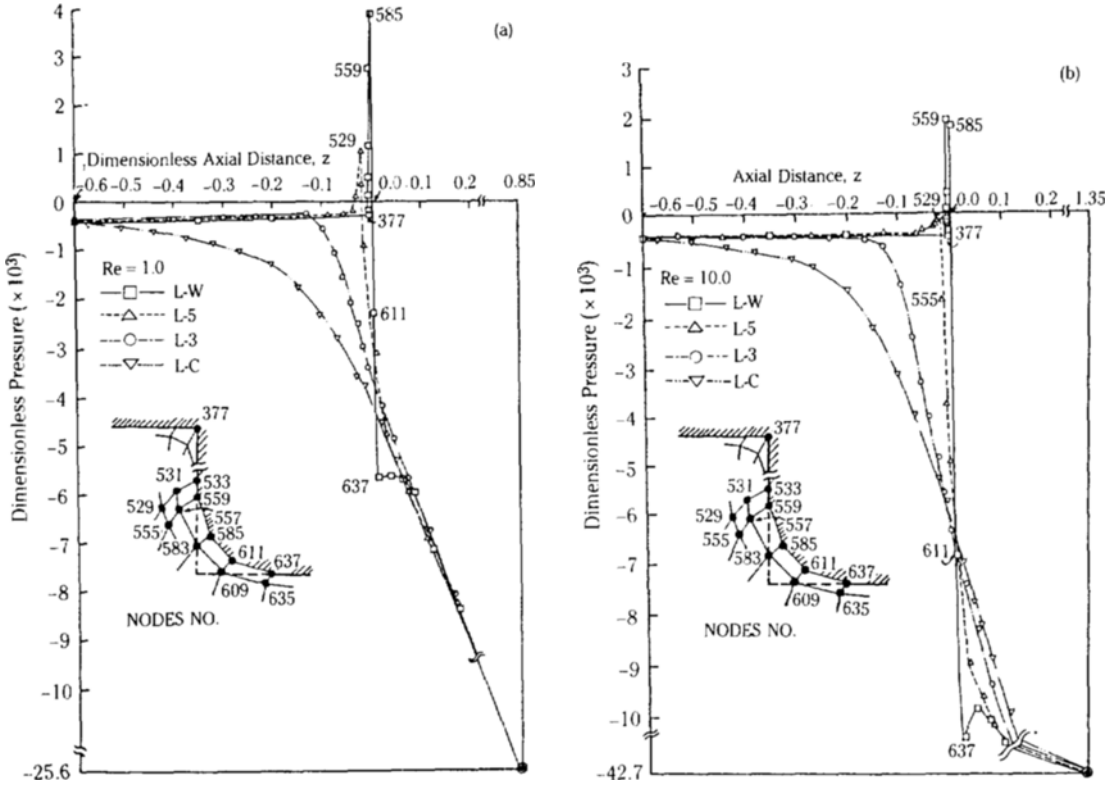

Fig. 8. Computed pressure profiles along the axis for mesh layers of (a) Re = 1.0 and (b) Re = 10.

nolds number. That is, at the higher Reynolds number the maximum occurs at the earlier node which is more toward the upper corner (number 559 instead of 585 at Re = 10 in our problem), while at the lower Reynolds number it takes place at the later node which is more toward the entry point (number 585 instead of 559 at Re = 1.0). This fact instructs us why the size and the strength of the vorticity are reduced with the high Reynolds number: for instance, it pushes the vorticity further up more into the corner by placing the maximum pressure closer to that region, but the less magnitude of its maximum relative to the lower Re may be associated with the weaker vorticity generated.

Referring to Figs. 8(a) and 8(b), it is seen that the sudden pressure drop at the node 637 reaches -5.8 for Re = 1.0 and -11.0 for Re = 10.0 relative to the zero value of the dimensionless pressure of the fully developed upstream (The pressure value here is meaningless and just gives the concept of the relative size). This implies that higher is the Reynolds number, more does the pressure drop to show further acceleration of the velocity.

In this view, the maximum pressure spot seems to divide the upper vorticity from the higher acceleration of the velocity field. Also, for the lowest sudden pressure drop at the node 637 which decreases beyond the corresponding value of the centerline is considered to be the velocity which surpass the center velocity. In other words, it is the location which gives the fastest velocity in the whole flow field.

The pressure drop along the centerline which has been depicted by the L-C layer in Fig. 8 may be the typical pressure decrease against the shear force induced by the flow because the centerline pressure is believed not to be under the influence of sudden contraction. The pressure above or below this curve may be regarded as the pressure loss or the gain respectively. Obviously, Fig. 8 demonstrates that the pressure loss (the rise) is further greater than the pressure gain (the drop). The net loss, then, is known to be the extra pressure loss due to the sudden contraction. It is also shown that the extra pressure loss of the low Reynolds number flow is greater than that of the high Reynolds number flow.

Finally, we want to mention that the entrance length of the flow disturbance due to contraction persists longer with high Reynolds number than with lower one. The constant pressure gradient developed in the downstream in the small tube is the indication of the end of the entrance length which has been started from the inlet. In our case, the entrance length z = 0.2 is required for Re = 1.0 and z = 1.35 for Re = 10.0 to reach the fully developed state, such as illusrated in Figs. 8(a) and 8(b).

CONCLUSION

A focal point of this study was to analyze the Navier-Stokes fluid flowing through a 4/1 contraction tube. From computational results, we have predicted in detail complex flow behaviors near the contraction point. For instance, the velocity and the pressure profile, the entrance length of the flow disturbance, the vortex generation with its size and strength, the extra pressure loss, the location of the fastest flow velocity, and the spot of the maximum pressure rise, etc. have been demonstrated with different Reynolds numbers. Their effects on different Reynolds numbers has been investigated, too, to see how Reynolds number generally affects flow conditions.

To prove the validity of this study, the experimental and the numerical outcome performed by others are compared with our results. This comparison demonstrates qualitatively a good agreement with each other.

For further works, present work provides a basis of solving the Navier-Stokes equation with the energy equation to analyze the nonisothermal flow behavior, in which the temperature effect on the flow can be under investigation. Additionally, because our effort is performed at relatively low Reynolds number, the opportunity to examine the given system at high Reynolds number also remains for the advanced numerical endeavor.

NOMENCLATURE

g : Gravitational acceleration
J : System Jacobian matrix
L : Total tube length
N : Number of nodes
n : Outer normal vector
P : Pressure
R : Tube radius
R : Element residual vectors
Re : Reynolds number
r : Radial coordinate
t : Time
V_r : Radial velocity
V_z : Axial velocity
z : Axial coordinate of the contraction tube

Greek Letters

Γ_r : Boundary of flow field for radial coordinate
Γ_z : Boundary of flow field for axial coordinate
δ : Standard deviation between two consecutive iterated solutions
η : A dimensionless coordinate of shape function

θ_β : Bilinear shape function
ϕ_α : Nine-node biquadratic shape function
ψ : Unknown vector of formulating variables
ξ : A dimensionless coordinate of shape function
Ω : Flow field

Subscripts

n : Iteration number
,r : First-order derivative with respect to r
,z : First-order derivative with respect to z
,zz : Second-order derivative with respect to z

Superscripts

e : Finite element under consideration
* : Indication of weighting function

REFERENCES

1. Huyakorn, P.S., Taylor, C., Lee, R.L., and Gresho, P.M.: *Computers and Fluids*, **6,** 25 (1978).
2. Kawahara, M. and Takeuchi, N.: *Computers and Fluids*, **5,** 33 (1977).
3. Donea, J., Giuliani, S., Laval, H., and Quartapelle, L.: *Comp. Meth. Appl. Mech. Eng.*, **30,** 53 (1982).
4. Leone, J.M., Jr. and Gresho, P.M.: *J. Comp. Phys.*, **32,** 167 (1981).
5. Gresho, P.M. and Lee, R.L.: *ASME-AMD*, **34,** 37 (1979).
6. Vrentas, J.S. and Duda, J.L.: *Appl. Sci. Res.*, **28,** 241 (1973).
7. Duda, J.L. and Vrentas, J.S.: *Trans. Soc. Rheol.*, **17,** 89 (1973).
8. Christiansen, E.B., Kelsey, S.J., and Carter, T.R.: *AIChE J.*, **18,** 372 (1972).
9. Viriyayuthakorn, M. and Caswell, B.: *J. Non-Newtonian Fluid Mech.*, **6,** 245 (1980).
10. Keunings, R. and Crochet, M.J.: *J. Non-Newtonian Fluid Mech.*, **14,** 279 (1984).
11. Boger, D.V.: "Circular Entry Flows of Inelastic and Viscoelastic Fluids" in Advances in Transport Processes, Vol. 2, John Wiley and Sons, N.Y., pp.43-104 (1982).
12. Gartling, D.K. and Becker, E.B.: *Comp. Meth. Appl. Mech. Eng.*, **8,** 51, 127 (1976).
13. Kawahara, M., Yoshimura, N., Nakagawa, K., and Ohsaka, H.: *Int. J. Num. Meth. Eng.*, **10,** 437 (1976).
14. Hood, P.: *Int. J. Num. Meth. Eng.*, **10,** 379 (1976).
15. Moffat, H.K.: *J. Fluid Mech.*, **18,** 1 (1964).
16. Pan, F. and Acrivos, A.: *J. Fluid Mech.*, **28,** 643 (1967).
17. Nguyen, H. and Boger, D.V.: *J. Non-Newtonian Fluid Mech.*, **5,** 353 (1979).